Chapter 1

Introduction

1.1 Motivation

Until a few years ago experimental phenomena like particle and energy transport in magnetically confined plasmas could not be reproduced satisfactorily by plasma theory. In the last years some improvement could be achieved, but there is still need for a more detailed understanding of the processes involved. For illustration, figure 1.1 shows a comparison of theoretical and experimental results for ion heat diffusivity at JET.

The knowledge of the plasma parameters, especially in the plasma edge, is very important for the understanding of the plasma confinement in magnetic traps. In toroidal magnetically confined plasmas one distinguishes between the core plasma and the scrape-off layer. The core plasma is the region of closed flux surfaces, the scrape-off layer is the region where magnetically confined particles can get into contact with the vessel. In limiter plasmas (figure 1.2, left illustration) this contact occurs at the limiter, in so-called X-point plasmas the particles hit a divertor (figure 1.2, right illustration). In both scenarios the magnetic field lines outside the separatrix, i.e. the last closed flux surface, connect into the wall. The term 'plasma edge' denotes the separatrix and the scrape-off layer.

Energy and particle transport through the plasma edge are crucial for both the properties of the core plasma and the power deposition onto the wall. For understanding of transport phenomena in the plasma edge and for the definition of the input parameters in transport codes a precise knowledge of the temperature- and density gradients is essential.

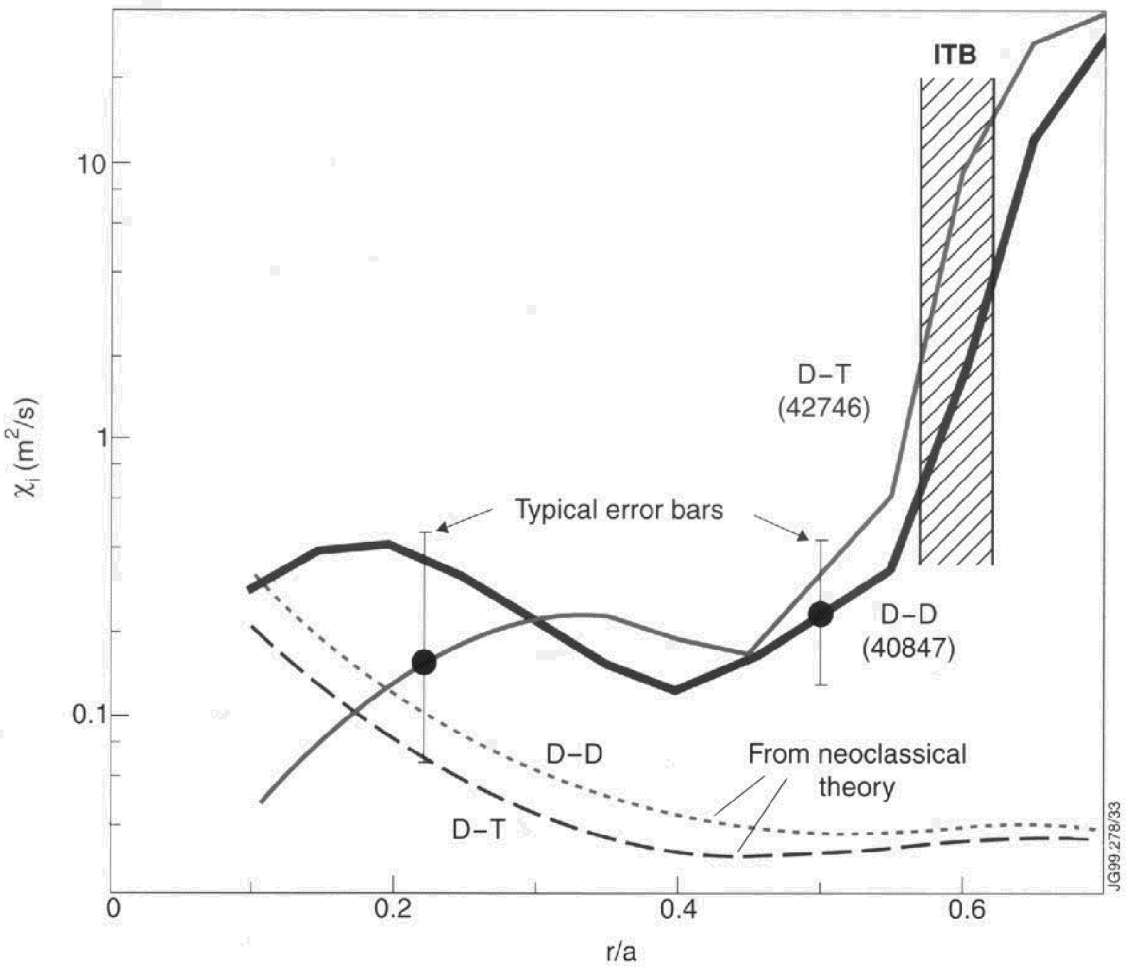

Figure 1.1: Radial ion thermal diffusivity profiles for typical optimized shear pulses in D-D- (discharge #42746) and D-T plasmas (discharge #40847) at JET [4].

Four different types of plasma confinement have been identified experimentally:

- L-mode confinement with smooth pressure profiles,
- H-mode confinement with reduced transport at the edge, leading to the formation of a so-called pedestal,
- ITB discharges in which an **i**nternal **t**ransport **b**arrier with a steeper pressure gradient is achieved by optimizing the current profile in L- or H-mode plasmas,
- RI-mode confinement where a transport barrier is produced by injection of impurities [6, 7].

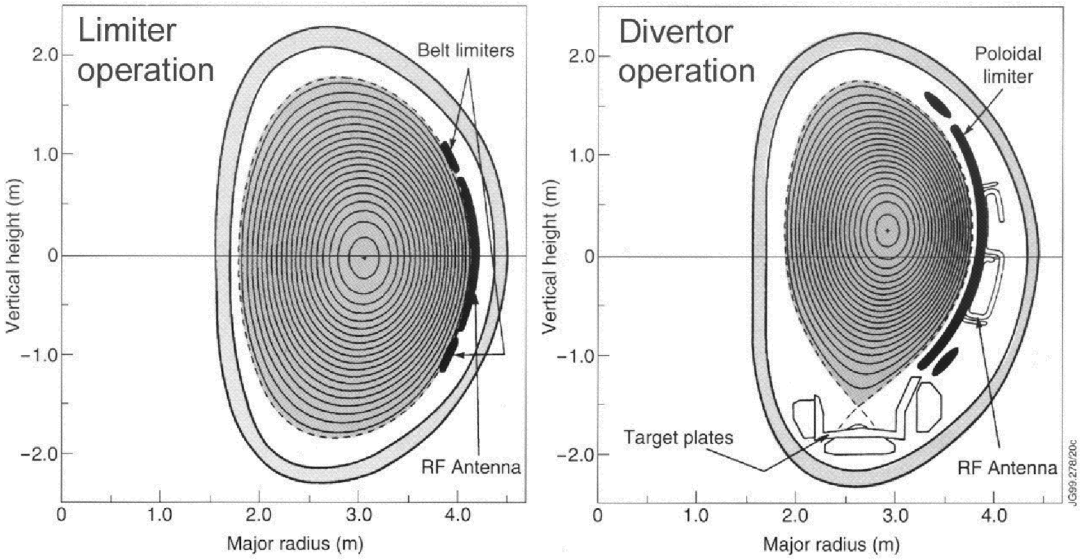

Figure 1.2: Schematic diagram of poloidal magnetic flux surfaces. Left: with a limiter, right: with a divertor ('target plates'). The concentric curves indicate the closed magnetic flux surfaces, the dashed line the separatrix [4].

The first three of these regimes are shown in figure 1.3. The change in temperature- and density profiles during the development of an ITB is illustrated in figures 1.4 and 1.5.

The formation of transport barriers has a dramatic effect onto plasma performance [9, 10]. Hence, for a detailed understanding of all processes affecting confinement, a precise knowledge of the temperature- and density gradients of both the edge transport barrier and the ITB is essential. However, no satisfactory method for a high local resolution measurement of these steep-parameter profiles, especially the temperature profiles (see figures 1.1 and 1.5), exists until now. Consequently, there is a strong interest in the development of diagnostics accommodating this demand. A newly developed method, fast He beam diagnostics, could be a suitable candidate for this. The aim of this work is to explore the diagnostic capabilities of fast He beams.

In the next chapters a survey of the most important diagnostic methods for the determination of plasma temperatures and -densities will be given. In chapter 1.3 the principle of fast He beam diagnostics is explained.

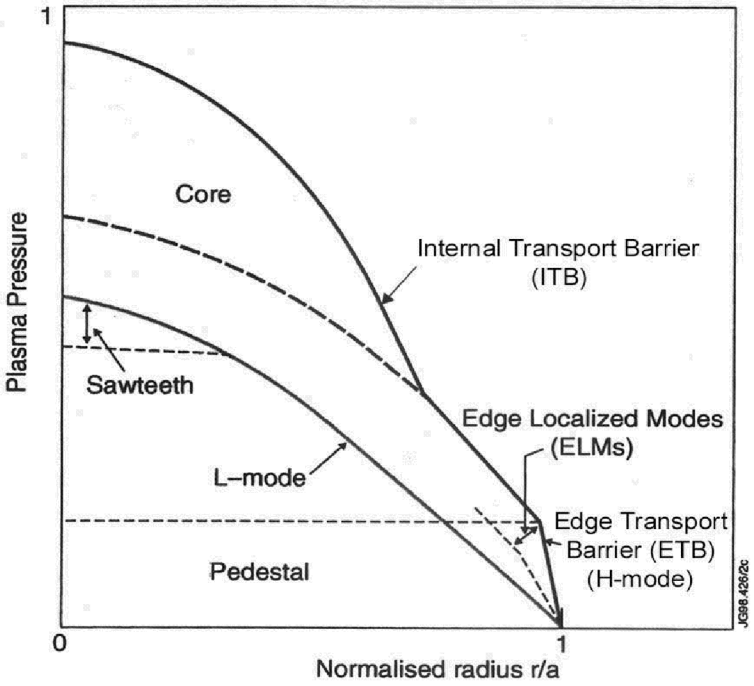

Figure 1.3: Normalized plasma-pressure profiles of L- and H-mode plasmas with and without internal transport barrier [5]. r stands for the major radius, a for the radial position of the separatrix (r/a=1).

1.2 Established Diagnostic Methods

The progress in fusion research over the last decade is not only measured by its success on the way to controlled fusion but also by the parallel development of novel diagnostic tools providing reliable and quantitative values of relevant plasma parameters. Because of the high temperatures in nowadays fusion plasmas, methods involving physical contact with the plasma can be used only at the outermost part of the discharge. Hence, for measurements in the plasma core, non-invasive techniques have to be used. Some methods are 'passive' and utilize particles or radiation that are emitted spontaneously by the plasma. 'Active techniques' use beams of particles or radiation from external sources as probes. The following diagnostic methods for determining electron- and ion density and -temperature are of relevance for present magnetically confined fusion experiments:

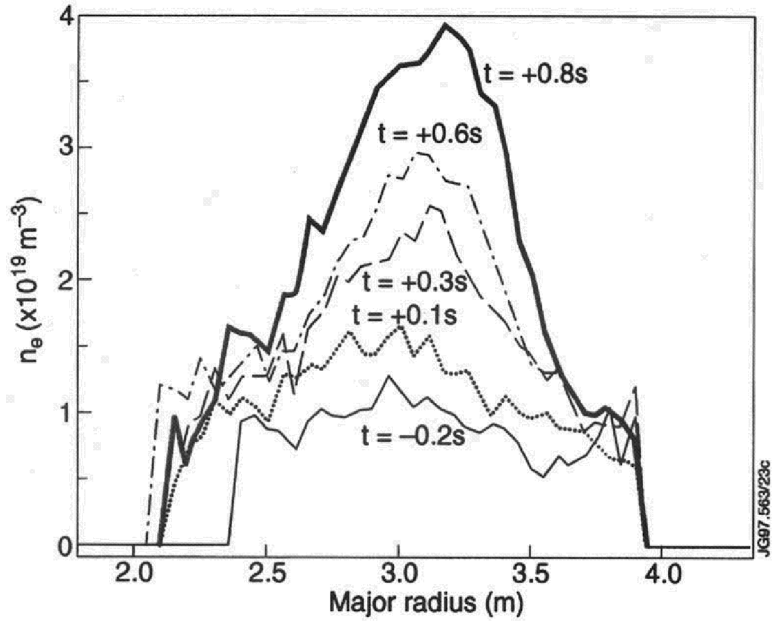

Figure 1.4: Change in electron-density profiles during the production of ITBs in a JET D-T plasma (discharge #42940) [8]. The separatrix is located at a major radius of about 3.85 m and 2.15 m, respectively.

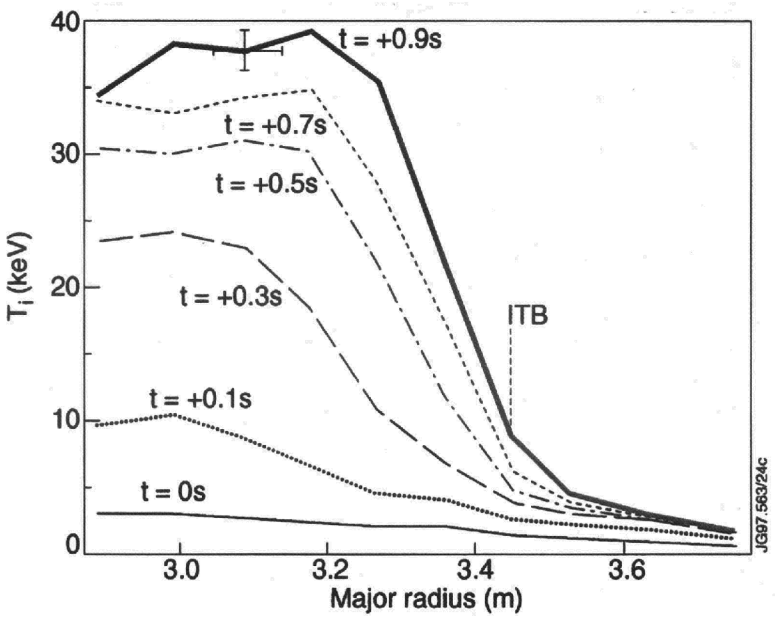

Figure 1.5: Change in ion-temperature profiles during the production of ITBs in a JET D-T plasma (discharge #42940) [8].

Langmuir probes
Thomson scattering
electron cyclotron emission (ECE)
reflectometry
interferometry
laser induced fluorescence
neutral particle analysis
neutral beam diagnostics (Li, fast H and D, and thermal He)

1.2.1 Langmuir Probes

This technique, developed by Irving Langmuir in the 1920s, is based on current measurements. In its simplest form, a Langmuir probe consists of a single electrode inserted into the plasma. A voltage is applied to the probe with respect to the vessel and the resulting current through the electrode is measured. From the current-voltage characteristics the electron density and -temperature at the position of the probe can be deduced.

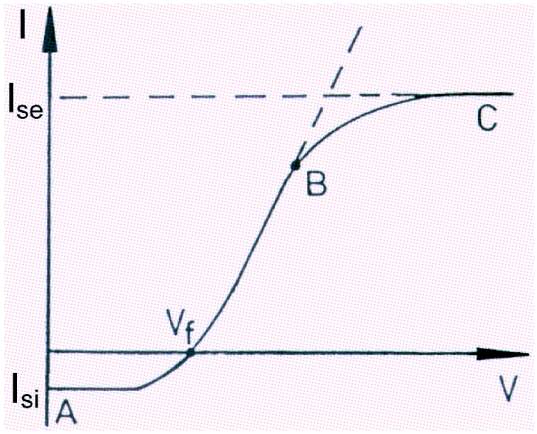

Figure 1.6: Current-voltage characteristics of a Langmuir probe [11], details are explained in the text.

Figure 1.6 shows the current-voltage characteristics of a Langmuir probe. V denotes the applied voltage, I the current through the probe, and V_f the floating potential which is reached when the net current is zero (if electrically isolated, the probe would float at this potential). The saturation current I_{si} is reached for strong negative voltage (all electrons are repelled), the electron saturation current I_{se} for strong positive voltage (all ions are repelled). The current-voltage profile between $I(V = 0)$ and I(B) (see figure 1.6) follows approximately

$$ln\,(I + I_{si}) \propto \frac{e\,V}{k_B\,T_e}\,. \tag{1.1}$$

where e denotes the elementary charge ($1.602{\cdot}10^{-19}$ C) and k_B the Boltzmann constant ($1.38{\cdot}10^{-23}$ J/K). Hence, the electron temperature T_e at the probe position can be determined by measuring V, I, and I_{si}. Assuming equal ion- and electron temperatures leads to the following correlation between I_{se} and the electron density n_e:

$$I_{se} = e\,n_e\sqrt{\frac{k_B\,T_e}{2\,\pi\,m_e}}\,S\,. \tag{1.2}$$

S stands for the projected surface area of the inner electrode seen by the plasma and m_e for the electron mass ($9.109{\cdot}10^{-31}$ kg). In magnetized plasmas, the measured I_{se} is much less than expected from theory. Only the tail of the electron distribution (about 5% of the total) is collected [12]. Nevertheless, n_e can be derived from measurement of I_{si} assuming equal T_i and T_e:

$$n_e = \frac{I_{si}}{e\,S}\sqrt{\frac{2\,\pi\,m_i}{k_B\,T_e}}\,, \tag{1.3}$$

m_i denotes the ion mass.

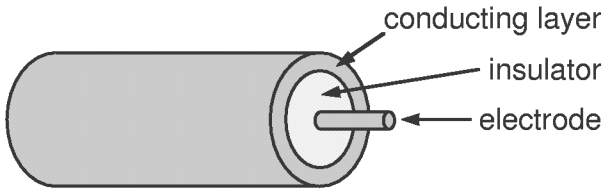

Figure 1.7: Schematic construction of a coaxial Langmuir probe.

Figure 1.7 shows a typical Langmuir probe of coaxial construction. It consists of an inner electrode made of heavy metal (e.g. platinum, molybdenum) sticking out of an isolating layer (e.g. alumina, quartz), which is shielded by a conducting layer.

The probes have to be in contact with the plasma and can only be used in areas where the power density is below the limit set by the probe material. The use of so-called 'reciprocating probes', i.e. an array of Langmuir probes which is only shortly inserted into the plasma edge (see figure 1.8), allows to extend the diagnostic region deeper into the plasma. However, the application of this type of probes is confined to plasma regions where $T_e \leq 100$ eV and $n_e \leq 10^{20}$ m^{-3}. At higher particle fluxes the probe would be destroyed leading to an increase

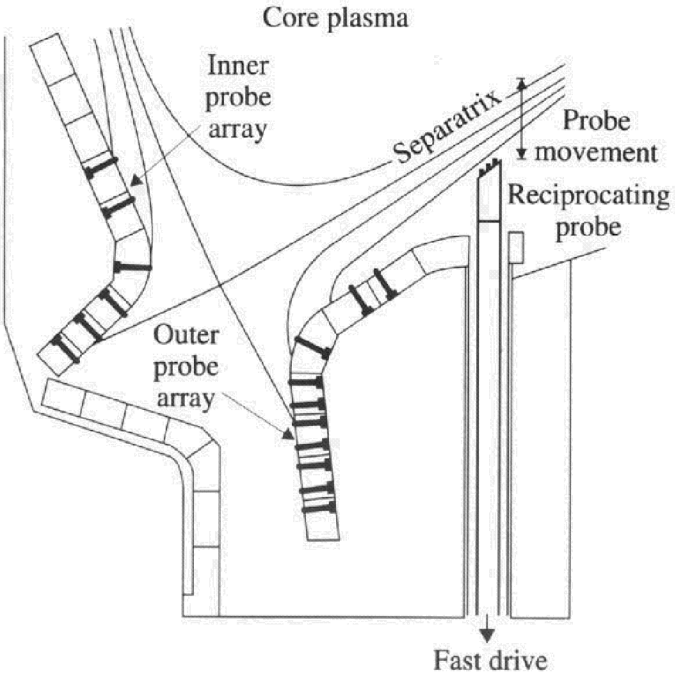

Figure 1.8: Fast reciprocating Langmuir probe and fixed Langmuir probe arrays in the divertor region of Alcator C-mod tokamak [12, 13].

of the impurity density and to undesired cooling of the plasma edge. Hence, the use of Langmuir probes inside the separatrix is fairly limited, even if installed on a reciprocating probe. An additional disadvantage of this diagnostic method is the difficult interpretation of the measured signals in the presence of high magnetic fields.

1.2.2 Thomson Scattering

Thomson scattering is used for measuring electron temperature- and density profiles by directing a laser beam into the plasma and detecting the scattered radiation.

Charged plasma particles hit by the laser light are accelerated and emit electromagnetic radiation like Hertzian dipoles. Being based on charge acceleration, this effect is much larger for electrons because of their smaller mass than for any other plasma particle. The differential cross section for Thomson scattering at an electron is given by

$$\frac{d\sigma}{d\Omega} = r_o^2 \, sin^2\theta = \left(\frac{e^2}{4\,\pi\,\epsilon_o\,m_e\,c^2} \right)^2 sin^2\theta\,, \tag{1.4}$$

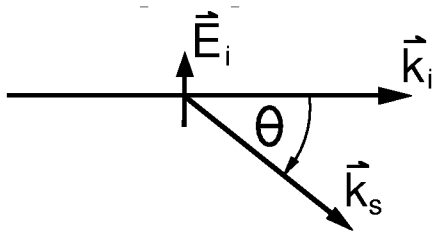

Figure 1.9: Definition of the scattering angle θ. $\vec{k_i}$ and $\vec{k_s}$ denote the wave vector of the incident and the scattered light wave, respectively, $\vec{E_i}$ stands for the electric field vector of the incident beam.

where Ω denotes the solid angle, r_o the 'classical electron radius' ($2.82{\cdot}10^{-15}$ m), θ the scattering angle (see figure 1.9), ϵ_o the electric constant ($8.85{\cdot}10^{-12}$ $\frac{As}{Vm}$), and c the speed of light ($2.998{\cdot}10^{8}$ m/s). Due to the high electron temperature T_e, a scattered line with wavelength λ_o exhibits Doppler broadening with a full width at half maximum of

$$\Delta\lambda = 4\,\lambda_o\,sin\left(\frac{\theta}{2}\right)\sqrt{\frac{2\,k_B\,T_e\,ln2}{m_e\,c^2}}\,, \tag{1.5}$$

which makes it possible to determine T_e. The scattered power P_s per unit angle θ in the frequency bandwidth $d\omega$ is given by

$$P_s = P_o\,n_e\,r_o^2\,sin^2\theta\,L\,S(k,\omega)\,d\omega\,, \tag{1.6}$$

where P_o denotes the total incident laser power, L the interaction length, and $S(k,\omega)$ the spectral density function. k stands for the magnitude of the difference between incident and scattered wave vectors and ω for the difference between scattered and incident frequencies [12]. The dependence of P_s on n_e allows the determination of the latter by measuring the differential scattered power, which requires a much higher laser power or a much better sensitivity of the detection system than needed in T_e measurements. At JET several of these Thomson laser beams are installed and used for real-time controlling of n_e [14].

As P_s depends on r_o^2 ($8{\cdot}10^{-30}$ m^2), the scattering effect is quite weak. In order to get signals from the scattering processes exceeding the background radiation, multimegawatt pulsed lasers (Nd:YAG or ruby lasers) and very sensitive detection systems have to be used. Figure 1.10 shows the technique usually termed 'Thomson scattering'. Here the scattered light is observed at angles close to perpendicular to the beam path. In another version of the Thomson scattering method called 'LIDAR' (**li**ght **d**etection **a**nd **r**anging) a pulsed

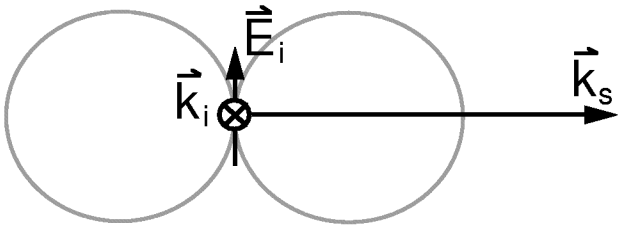

Figure 1.10: Principle of Thomson scattering measurements with observation perpendicular to the laser beam. $\vec{k_i}$ and $\vec{k_s}$ denote the wave vector of the incident and the scattered beam, respectively. $\vec{E_i}$ stands for the electric field vector of the incident beam.

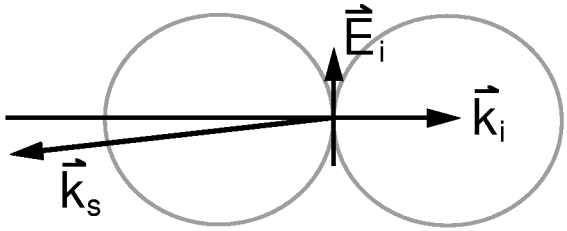

Figure 1.11: Principle of LIDAR measurements. $\vec{k_i}$ and $\vec{k_s}$ denote the wave vector of the incident and the scattered beam, respectively. $\vec{E_i}$ stands for the electric field vector of the incident beam.

laser is used and the backscattered light is recorded as function of time by a fast detection and recording system. As the laser pulses are rather short, the position of the laser photon packet is known at each time point. LIDAR uses the time of flight of this short laser pulse to spatially resolve the n_e and T_e data. Figure 1.11 shows the geometry for this diagnostic. At the LIDAR system at JET the pulse duration is 300 ps (9 cm wave packets) and the repetition rate 4 Hz. With this system a local resolution of 5 cm could be achieved [15].

Thomson scattering systems observing perpendicular to the incident laser beam require at least two approximately orthogonal views, i.e. one for the incident beam and another for the observation system. The latter has to allow wide angle observations (see figure 1.12). LIDAR requires only a single line of sight access to the plasma, which makes this kind of diagnostic more favourable for future fusion devices. Nevertheless, all temperature profiles of transport barriers determined by Thomson scattering or LIDAR known to the author (e.g. figure 1.5) are characterized by low spatial resolution and do not allow evaluation of detailed T_e profiles.

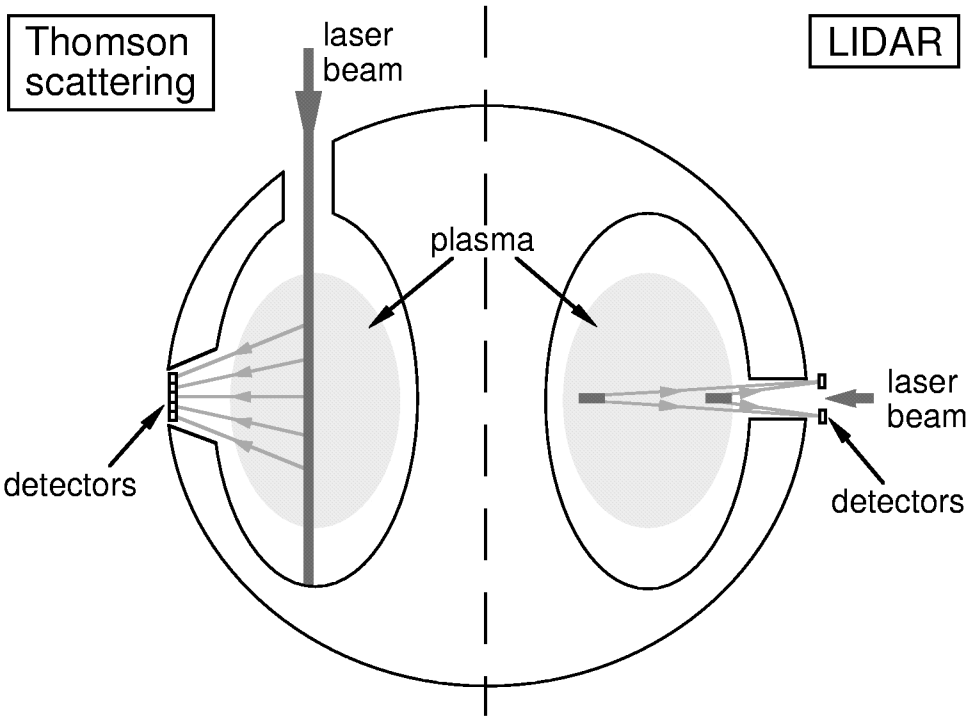

Figure 1.12: Schematic view of the Thomson scattering and the LIDAR system installed at JET.

1.2.3 Electron Cyclotron Emission (ECE)

This passive diagnostic method makes use of the electron gyration in a magnetic field. During this acceleration movement the electrons emit radiation at frequencies ω corresponding to the electron cyclotron frequency ω_{ce} and its harmonics

$$\omega = l\,\omega_{ce} = l\,\frac{e\,B}{m_e}, \tag{1.7}$$

where l (l = 1,2,3...) denotes the harmonic number and B the local magnetic field. Under some circumstances, the intensity of the emission is directly related to T_e. In the general case the calculation of the electron cyclotron emission of a plasma is extremely complicated. Even for the simplified case of a plasma with Maxwellian velocity distribution and electron densities $n_e \leq 10^{20}$ m^{-3}, the emission $j(l\,\omega_{ce})$ is a rather complicated function of T_e, l, and of the angle θ between the direction of the emission and the confining magnetic field [12].

This correlation becomes very simple if the plasma is optically thick for the frequency ω under consideration. This means that the optical depth $\tau(\omega)$, an absolute measure of the

plasma for this frequency defined by

$$\tau(\omega) = \int \alpha(\omega, s)\, ds\,, \tag{1.8}$$

should be larger than 1. In equation 1.8 $\alpha(\omega, s)$ stands for the absorption coefficient of the wave in the plasma which has to be integrated along the line of sight (line parameter s). In this case, the wave gets re-absorbed in the plasma and the radiation intensity becomes that of a blackbody. For typical Tokamak experiments ($2\,T \leq B \leq 8\,T,\ 5\,mm \geq \lambda \geq 0.5\,mm$), the emission lines of interest are on the long wavelength side of the blackbody spectrum ($h\nu \ll k_B T_e$). Hence, the Rayleigh-Jeans law holds,

$$I_n(\omega) = \frac{\omega^2\, T_e}{8\,\pi^3\, c^2}\,, \tag{1.9}$$

allowing the calculation of T_e from the measurement of the intensity $I_n(\omega)$ of the emission of an optically thick harmonic.

The fundamental wave is absorbed at the upper hybrid resonance with the frequency

$$\omega_{uh} = \sqrt{\omega_{pe}^2 + \omega_{ce}^2} \approx \omega_{ce}\,, \tag{1.10}$$

where

$$\omega_{pe} = \sqrt{\frac{n_p\, e^2}{\epsilon_o\, m_e}} \tag{1.11}$$

denotes the electron plasma frequency. Thus, the fundamental wave can not be detected. Consequently, the second harmonic ($\omega = 2\,\omega_{ce}$) is commonly chosen for the measurement.

The magnetic field B of a Tokamak varies inversely with the major radius R. Consequently the electron cyclotron frequency shows the same $1/R$ behaviour. This means that the frequency of the emission can be used to deduce the radial location of the source of the emission and, hence, the spatial T_e profile can be deduced. The spatial resolution is typically a few cm, which limits the local resolution for high T_e gradients.

There are several effects that can limit the usefulness of this diagnostics, such as deviation of the velocity distribution from Maxwellian, plasma currents which generate an additional magnetic field, refraction of the emission light, and density effects which change the propagation properties. Due to large variations of the magnetic field in the plasma, two or even more harmonics may be resonant at the same frequency at different radii ('harmonic overlap').

Comparison of results for T_e from ECE and Thomson scattering measurements show that the derived ECE data are reliable for $T_e \cdot n_e \geq 3 \cdot 10^{18}\,\mathrm{keV\,m^{-3}}$. Below this plasma pressure the optical depth is decreased to such an extent that the plasma can not be considered a blackbody any more. Hence, the simple correlation between T_e and $I_n(\omega)$ given above does not hold any longer. Effects like the reflectivity of the inner wall of the plasma vessel become important. Measurements during H-modes with very steep edge T_e gradients and low densities showed enhanced emission (local maximum of T_e outside the separatrix). This phenomenon is not fully understood until now, an explanation could be a non-thermal electron velocity distribution due to enhanced transport of fast electrons in this region [16].

1.2.4 Reflectometry

A beam of microwave radiation is directed into the plasma and reflected at the density layer where the local electron density is equal to the cut-off density (cf. equ. 1.11) which is a function of the wave frequency. By sweeping the frequency, the electron-density profile can be determined.

The refractive index N for a so-called 'ordinary' electromagnetic wave (electric vector parallel to magnetic field) with the frequency ω is given by

$$N = \sqrt{1 - \frac{\omega_{pe}^2}{\omega^2}} = \sqrt{1 - \frac{n_e\, e^2}{\epsilon_o\, m_e\, \omega^2}}\,. \tag{1.12}$$

At the location where the electron density exceeds the critical density

$$n_c(\omega) = \frac{\epsilon_o\, m_e\, \omega^2}{e^2} \tag{1.13}$$

an electromagnetic wave of the frequency ω can not propagate any more and thus becomes reflected.

Using a Michelson interferometer, the phase shift between the incident and the reflected wave can be measured, which makes it possible to determine the position of the corresponding $n_c(\omega)$ layer (so-called 'cut-off layer') as shown in figure 1.13. By tuning the laser frequency the electron-density profile can be measured. The accessible density area is limited by the frequency range of the tuneable microwave source. E.g. at JET the reflectometer used covers the density range $4{\cdot}10^{18}$ m^{-3} to $8{\cdot}10^{19}$ m^{-3} [12]. Furthermore, only monotonously increasing density profiles can be measured, and the measurements can be disturbed by local density fluctuations.

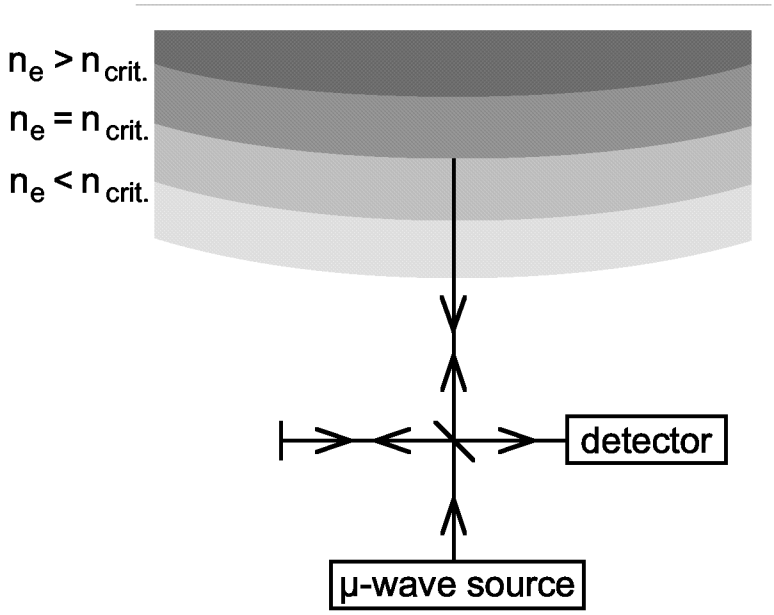

Figure 1.13: Schematic diagram of a reflectometer for determining n_e profiles.

1.2.5 Interferometry

Transmission interferometry is one of the oldest established diagnostic methods for measuring the electron-density profile. A laser beam is split by semipermeable mirrors into several coherent waves which are directed through the plasma (see figure 1.14). From the phase shifts of the single beams the electron-density profile can be deduced. In this case the laser frequency has to be higher than the maximum plasma frequency in the region of interest. Therefore, usually lasers with frequencies in the far infrared, e.g. HCN-lasers, are employed.

The difference of the phases of a beam with frequency λ passing through a plasma and those of the reference beam is proportional to the electron density integrated along the beam path [12]:

$$\Delta\phi = \frac{\lambda\, e^2}{4\,\pi\,\epsilon_o\, m_e\, c^2} \int n_e\, dl\,. \tag{1.14}$$

These phase shifts can be measured, e.g. with a Michelson interferometer. From the known phase shifts, electron-density profiles can be deduced by tomographic inversion (Abel inversion). Multiple lines of sight through the plasma would be required in order to measure detailed plasma-density profiles. This appears to be extremely difficult to implement in a device such as ITER, i.e. the next major step for the development of nuclear fusion [17].

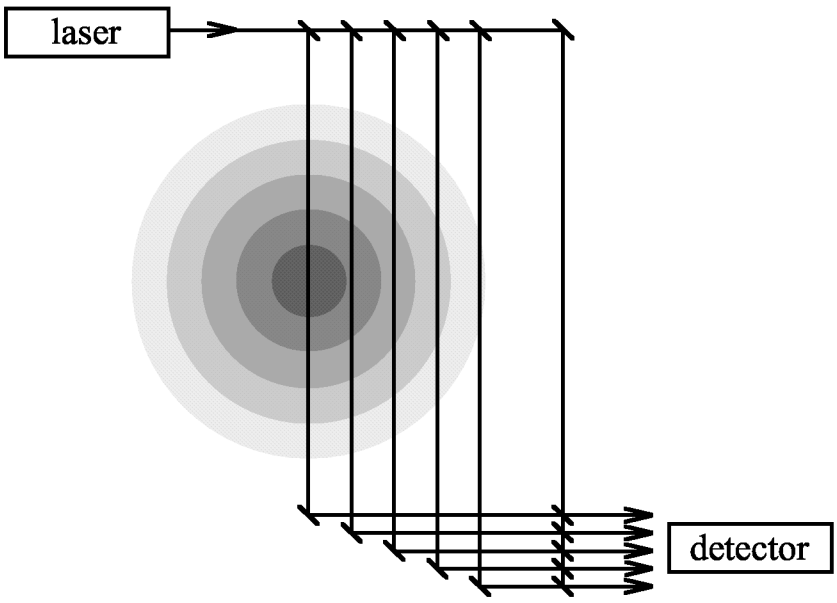

Figure 1.14: Schematic layout of an interferometer used for n_e measurements.

Even at JET there are insufficient lines of sight (5 vertical and 3 horizontal) to yield density profiles with good spatial resolution. Furthermore, interferometry systems are very sensitive to mechanical vibrations. In order to decouple from the tokamak, the interferometer at JET is mounted on a large, independently supported frame. For ITER such a frame would be impracticably large. Hence, the use of interferometry as major diagnostics for density-profile measurements at ITER is questionable [18]. From that point of view, reflectometry seems preferable, as the measurements are done by probing the plasma along a single line of sight.

1.2.6 Laser Induced Fluorescence (LIF)

In a fusion plasma, there is often a difference between T_i and T_e because the ion-electron equilibration time can become comparable to or even longer than the ion energy confinement time. This is especially the case for auxiliary-heated discharges (RF- or neutral beam heating). Hence, a dedicated diagnostic method for determining the temperature of ions is of high interest. LIF is a method for measuring temperature and density of atoms and non fully stripped ions.

In LIF, laser light of a frequency equal to the excitation frequency of the atom or ion of interest is directed through the plasma. The intensity and Doppler broadening of the fluorescent radiation emitted by the excited particles gives access to the density and temperature

of the latter. One of the most important applications of LIF is the Lyman-α-fluorescence. Here, laser light of the frequency 121.6 nm is used to excite hydrogen atoms into their first excited level (n=2). This diagnostic requires neutrals or non-fully stripped ions, and is therefore rather limited. Nowadays, this diagnostics - no longer in use at the most important fusion experiments - has been replaced by neutral particle analysis and neutral beam charge-exchange spectroscopy.

1.2.7 Neutral Particle Analysis

This method makes use of fast neutrals escaping the plasma for determining ion-temperature profiles. Plasma neutrals have their origin either on the vessel wall or in low-charged ions recombining with other plasma particles. These slow neutrals are not confined by the magnetic field and, therefore, can either escape from the plasma or penetrate deeper into the plasma where a charge-exchange process with a plasma ion leads to a secondary neutral, and so on. By this process at low densities the hydrogen atoms can penetrate into the plasma center [12]. Hence, measurements of escaping neutrals give access not only to parameters of edge ions but also of core ions.

The neutral flux escaping a Maxwellian plasma is given by

$$S(E_o) = n_o\, n_i\, \langle \sigma_{01} v_i \rangle \, \frac{2\sqrt{E_0}}{\sqrt{\pi}\,\sqrt[3]{k_B T_i}}\, e^{\frac{E_o}{k_B T_i}}\,, \tag{1.15}$$

where E_o stands for the energy of the neutrals, n_o and n_i for the density of the neutrals and ions, respectively, and σ_{01} for the charge-exchange cross section. If n_i is known, the measurement of $S(E_o)$ gives access to T_i and n_o. One prerequisite for the applicability of equation 1.15 is that the mean free path of the escaping neutrals has to be much greater than the plasma radius a,

$$\frac{1}{n_i\, \sigma_{01}} > a\,, \tag{1.16}$$

which is correct for higher energies as σ_{01} decreases with increasing energy.

In the detection system the neutral particles are ionized in a gas stripping cell or thin carbon foil and afterwards analysed due to their energy and mass. The detected values for T_i and n_o are line-of-sight averaged. Thus, for the determination of radial profiles of these parameters, the measured values have to be interpreted by rather complicated plasma modelling [19]. Due to the complexity of these calculations, the results are - under some circumstances -

not very reliable. Application at small and medium tokamaks was quite successful but, for larger tokamaks, these measurements become less feasible because neutrals produced in the plasma center are ionized before leaving the plasma [12].

1.2.8 Neutral Beam Diagnostics

Neutral beams injected into the plasma are widely used for active spectroscopic measurements of key plasma parameters (see e.g. [20]). Two processes between beam atoms (B^o) and plasma particles (A^q, e) are important, i.e. charge-exchange reactions between beam atoms and plasma ions which in general lead to excitation of the latter,

$$B^o + A^q \rightarrow B^+ + (A^{q-1})^* , \tag{1.17}$$

and the excitation of the beam atoms themselves by collisions with electrons and ions,

$$B^o + A^q, e \rightarrow (B^o)^* + \dots . \tag{1.18}$$

Spectroscopy based on observing photons emitted by the plasma ions (or neutrals) is called 'charge-exchange spectroscopy' (CXS), observation of photons emitted by the beam atoms is termed 'beam emission spectroscopy' (BES) or 'impact excitation spectroscopy' (IXS). From the intensity of the CXS emission lines - determined by the density of the plasma ions, the flux density of the neutral beam, and the respective cross sections - the ion density can be deduced if the beam attenuation and the cross sections are known. Ion temperature and plasma rotation can be derived from width and Doppler shift of the spectral line. As these diagnostics are based on charge exchange, they enable the deduction of the parameters mentioned above even for fully ionized ions, in contrast to LIF. BES gives access to electron density and -temperature (see chapter 1.2.8.2), but also the local magnetic field (see chapter 1.2.8.1).

1.2.8.1 Hydrogen and Deuterium Beam Diagnostics

Hydrogen or deuterium heating beams are widely used also for plasma diagnostics [21, 22]. One very important application of H and D beams is the investigation of fusion alpha particles (i.e. CXS) [23]. As mentioned above, the neutral-beam density on the beam path has to be determined. In principle, two methods serve this purpose. The first one involves the direct measurement of the Balmer-α emission of the excited beam atoms. Then with the use

of atomic modelling to evaluate effective Balmer-α emission coefficients, the local neutral-beam density can be recovered. The second method is based on a numerical calculation of the attenuation along the beam path, which takes into consideration the atomic processes which contribute to ionizing the beam neutrals [24]. Presently, the spectroscopic method is the more accurate one, although it has proved difficult for several reasons. Firstly, the observed D_α emission is disturbed by Doppler shifts and the motional Stark effect in the magnetic field $\vec{B}$ caused by the Lorentz field

$$\vec{U}_L = \vec{v}_b \times \vec{B}\,, \tag{1.19}$$

where $\vec{v}_b$ denotes the velocity of the beam atoms. Furthermore, D (or H) beams have unwanted fractional energy components due to the production of these beams. In the beam source D_2 gas is ionized and D^+, D_2^+, and D_3^+ (D^++D_2) are formed and accelerated by an electric field. After acceleration the ions are neutralized and dissociated in a gas cell. Neutrals from dissociated D_2^+ have only one half and those from D_3^+ have only one third of the full energy. These fractional energy components in the atom beam leads to a superposition of the single Stark multiplets. Hence, the interpretation of these spectra is complicated by a large number of fits [24].

The spectral shape of the Balmer-α line can also be used for deduction of the total magnetic field perpendicular to the neutral beam, and the polarization of the line gives access to the pitch angle of the local magnetic field [22].

A disadvantage of D beams besides the complexity of the spectra is the high neutron production from beam-beam and beam-plasma interactions [25]. These neutrons contribute to the activation of the vessel [14].

1.2.8.2 Lithium Beam Diagnostics

Lithium beams of ≈ 0.1 eV (thermal beams produced with an oven, [26]), several eV (laser blow-off technique, [27, 28]) or several 10 keV and some mA equivalent current (produced by neutralizing a Li ion beam [3]) may be injected into the plasma. The emission of the Li(2p$\rightarrow$2s) transition gives access to the electron density (Li-IXS [29]) and the emission of excited impurity ions makes it possible to determine the temperature- and density profiles of the latter (Li-CXS [30]). The basis of the interpretation of the observed Li-IXS spectra is a collisional-radiative model which includes all relevant processes between the Li atoms and the plasma particles. As the rate coefficient for electron-impact excitation of Li is almost

independent of the electron temperature in the range of the accessible diagnostic region (several eV to several 100 eV), the exact profile of T_e can be neglected and the determination of n_e out of the diagnostic measurements is simplified considerably. But this also means that T_e can not be measured by Li beam diagnostics.

Li beam diagnostics enables spatial resolutions of about 5 mm [3], which is sufficient for the determination of detailed edge gradients. But due to the low ionization energy of Li, i.e. 5.39 eV, the beam does not penetrate far beyond the scrape-off layer in dense plasmas of nowadays tokamaks. Even fast lithium beam diagnostics is confined to the plasma edge and the outermost part (few cm) of the core plasma. Moreover, the error of n_e values rises for increasing penetration depth [3] due to the beam attenuation which results in decreasing signal intensities.

Figure 1.15 shows a typical H-mode n_e profile determined by Li-IXS in the plasma edge and by DCN-laser interferometry in the core plasma at ASDEX Upgrade. None of the diagnostics covers the pedestal region. This illustrates that a diagnostic covering both the edge transport barrier region and parts of the plasma inside the pedestal is desirable.

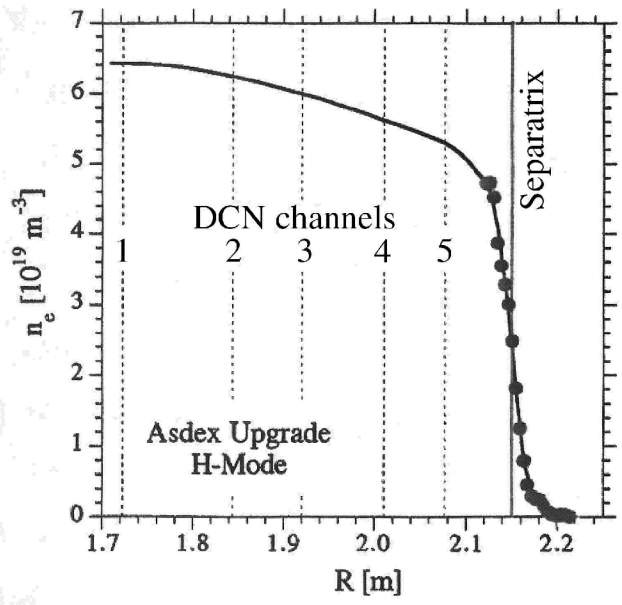

Figure 1.15: Typical H-mode n_e profile at ASDEX Upgrade. The broken lines denote the radial positions of the 5 DCN-laser interferometry channels, the circles denote the Li-IXS measurements [31].

This problem in the pedestal region gets worse for larger tokamaks (see figure 1.16 as an example for JET), especially for future devices, as the line integrated density rises.

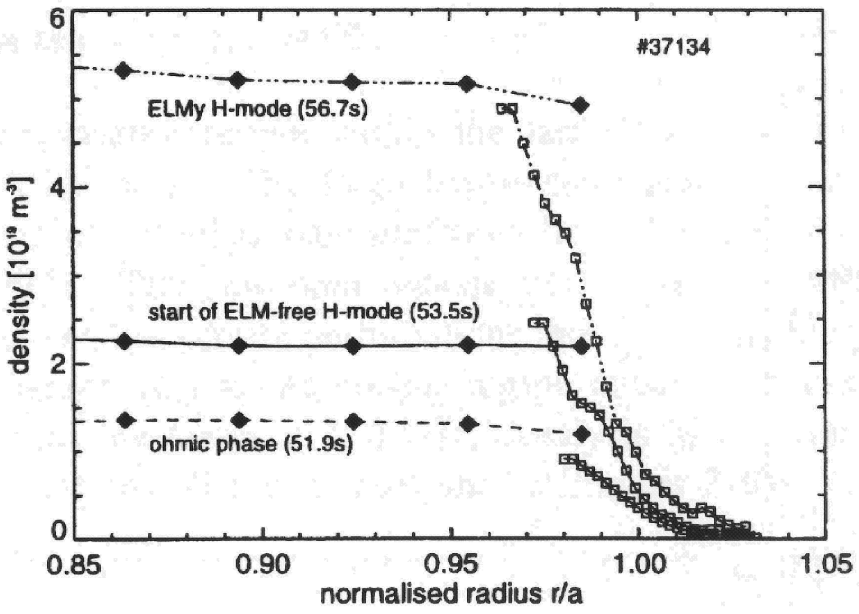

Figure 1.16: Density profiles for three different phases of a JET discharge. The black diamonds denote LIDAR measurements, the open squares Li beam diagnostics results [9].

1.2.8.3 Thermal Helium Beam Diagnostics

Thermal He beams - produced in an oven or by supersonic expansion through a nozzle - are injected into the plasma edge. At these beam energies the cross sections for reactions between the beam atoms and plasma ions can be neglected, see chapter 3.1. Neutral He has two different spin systems, i.e. singlet and triplet. The triplet system can only be populated from the He ground state by spin-changing processes. The different electron-temperature behaviour of the excitation cross sections for spin-conserving and spin-changing collisions gave rise to expectation, that the line-intensity ratio of a HeI-singlet and a HeI-triplet line should give access to the electron temperature [32]. On the other hand, the line-intensity ratio of two singlet lines can be used for the determination of the electron density. The deduction of n_e and T_e from line-intensity ratios is possible for thermal beams as the relevant excited levels are relaxed in typical tokamak discharges [33, 34]. Extensive calculations with a collisional-radiative model (cr-model, see chapter 3.2) make it possible to identify the most suitable ratios.

At TEXTOR, the ratio of the HeI emission at 728 nm ($3^1S \rightarrow 2^1P$) and at 707 nm ($3^3S \rightarrow 2^3P$) has been chosen for T_e measurements. The electron density is accessed by determining the ratio of the HeI emission at 728 nm and at 668 nm ($3^1D \rightarrow 2^1P$). Figure 1.17 shows the line-intensity ratios for 728 nm/707 nm and 668 nm/728 nm in the n_e-T_e-plane which are

used for the deduction of the n_e- and T_e profiles at TEXTOR [36].

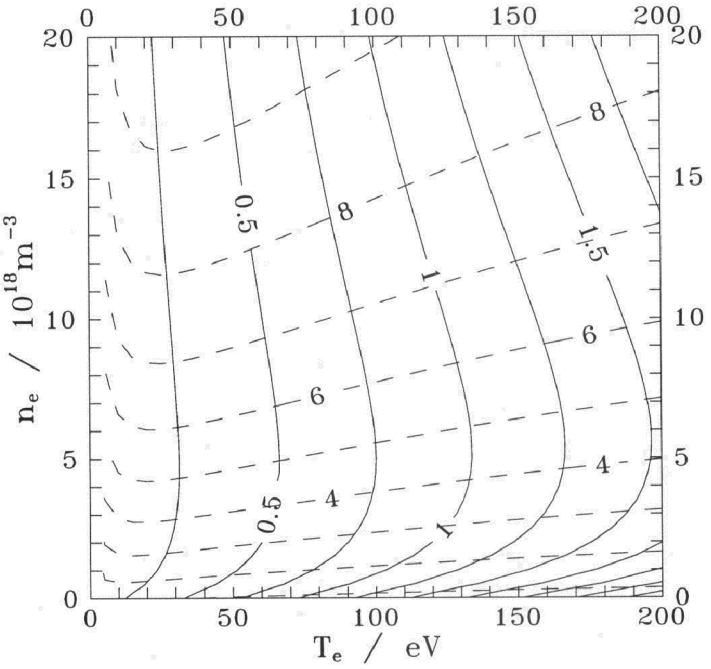

Figure 1.17: Line-intensity ratios for 728 nm/707 nm (solid line) and 668 nm/728 nm (broken line) in the n_e-T_e-plane for the deduction of the n_e- and T_e profiles [36].

Based on calculations performed with the cr-model by Fujimoto [34], several ratios of the emissions at 502 nm ($3^1P \rightarrow 3^1S$), 505 nm ($4^1S \rightarrow 2^1P$), 492 nm ($4^1D \rightarrow 2^1P$), and 471 nm ($4^3S \rightarrow 2^3P$) have been investigated at the NAGDIS-I linear plasma device (Nagoya University Divertor Simulator, [35]). The recommended line-intensity ratios are 492 nm/505 nm for the deduction of n_e and 505 nm/471 nm for T_e, respectively.

As the thermal He beams are ionized rather quickly, their diagnostic region is confined to the plasma edge (10^{18} m^{-3} $< n_e < 2 \cdot 10^{19}$ m^{-3} and 20 eV $< T_e <$ 200 eV [36]). A more detailed description of the diagnostic application and modelling of thermal He beams is given in chapter 3.1.

Summarizing the implementation of the methods described above, it is evident that there is considerable need for a method which allows to expand the diagnostic region deeper into the plasma than Li- or thermal He beams. This will be of special importance in view of future fusion devices which will involve much higher line integrated densities than the present ones. Furthermore, a more precise evaluation of T_e and n_e in plasma regions exhibiting high

gradients is desired. In the following chapter a new kind of plasma diagnostics using fast helium beams is presented, which seems to be a candidate for serving these purposes.

1.3 Fast Helium Beam Diagnostics

We assume that a neutral He beam of several 10 keV energy is injected into the plasma. As in the other neutral beam diagnostics mentioned above, observation of the HeI-line profiles should give access to the local n_e- and T_e profiles (BES). In addition, the emission lines of plasma-impurity ions which are excited via charge exchange with neutral He, may permit measurement of n_i and T_i (CXS). Furthermore, the resonant process of double charge exchange between ground-state He-beam atoms and plasma alpha particles enables the direct observation of the fast alpha particles (active neutral particle analysis [37]). As with Li beam diagnostics, a spatial resolution of several mm should be achievable.

Due to the high ionization energy of He atoms, fast He beams penetrate much deeper into the plasma than thermal He beams or fast Li beams. As with H or D beams, He beams could cover both the scrape-off layer and the core region. Besides the advantage of determining also n_e and T_e, neutral He beams produced by neutralizing a fast He-ion beam do not have fractional energy components as He does not form ionic molecules, and the He^{2+} fraction in the primary ion beam is negligibly small. Furthermore, He is not neutron producing - unlike deuterium.

Concerning CXS, the ground state helium atoms would be the primary donors for the $He^{+}(n = 4 - 3)$ emission lines, whereas $He(2^3S)$ metastable atoms would be primary donors for charge-exchange reactions like $C^{6+} \rightarrow C^{5+}(n = 8 - 7)$. Hence, for observation of the latter a high $He(2^3S)$ metastable fraction in the beam would be advantageous. In view of that application of He beams, so-called fast 'mixed' He beams, i.e. He beams with a high $He(2^3S)$ metastable fraction, were produced and characterized with regard to their composition in the first part of this thesis (chapter 2). These experiments were carried out at a 2.45 GHz ECR ion source of Institut für Allgemeine Physik (IAP). Also, the motional Stark effect on the $n \leq 3$ He levels is minimal. Hence, the $He(n = 3 \rightarrow 2)$ visible lines are not affected. This process becomes essential only for $n \geq 4$ shells, which in combination with the non-degenerate term structure of He may lead to the appearance of Stark induced forbidden lines [38]. This effect can be used for the determination of the internal magnetic field.

For quantitative interpretation of the observed line intensities, an extensive cr-model (see chapter 3.2) involving all collisions of importance between beam atoms and plasma particles had to be used. In contrast to the model used for thermal He beams, the ion-impact cross sections can not be neglected in comparison to the electron-impact cross sections (see chapter 3.1).

The line emission of fast He atoms inside a plasma has been modelled previously by several groups. Levinton [39] and Korotkov and Samsonov [40] developed a cr-model with the simplification of the metastables being in equilibrium relative to the ground state. This assumption was acceptable in view of calculating the attenuation of the He beam, as the most important process for ionizing the beam is ionization out of the ground state. This approach was continued by later work of Korotkov [41]. The population of each orbital-momentum substate of the low lying levels are evaluated, with the populations of the higher levels calculated for each principal quantum shell (nls-resolved/ns-resolved, cf. chapter 3.3). Korotkov and Janev [42] extended this work by using approximate methods to include metastable states of He. Brix [92] upgraded his cr-model for thermal He beams with proton impact- and charge-exchange cross sections. This model takes into account all levels up to $n = 5$.

During the last few years, a cr-model for He beams has been developed by the ADAS group at the University of Strathclyde, Glasgow [1], which is capable of calculating the He beam attenuation and excited state population structure. This is done by assembling effectively an infinite series of coupling equations (describing the population and depopulation of the single levels) with a varying resolution of substate populations [43]. The main part of this thesis presents modelling calculations based on this cr-model in order to investigate the diagnostic potential of a fast He beam. In chapter 3 the cr-model and the ANSI/C-code developed at IAP are described, which determine the population progression of the ground state and the two metastable states in the He beam, and resulting line-intensity profiles for optical lines of interest. In chapter 3.7 a survey of different methods for recalculating the electron density and -temperature from the observed emission lines is given. In order to make predictions for upcoming first experiments with fast He beams at Tokamak plasmas, calculations have been performed for He beams with various metastable fractions using electron density- and -temperature profiles typical for ASDEX Upgrade- and JET plasmas (chapter 4.1). Furthermore, the sensitivity of the line profiles to changes in electron density and temperature was analysed as presented in chapter 4.2. The last part of the present thesis - chapter 5 - deals with first relevant experiments performed at ASDEX Upgrade and JET, by which the results of these model calculations are compared with the experimental observations.